# Performance Enhancement of the DPC Control Based on a VGPI Controller Applied to a Grid Connected PV System

Mohamed Boukhalfa
LAADI Laboratory
Faculty of Science and Technology
University of Djelfa
Djelfa, Algeria
med.boukhalfa18@gmail.com

Amar Benaissa
LAADI Laboratory
Faculty of Science and Technology
University of Djelfa
Djelfa, Algeria
benaissa_am@yahoo.fr

Mohamed R. Bengourina
Centre de Développement des Energies Renouvelables
Algiers, Algeria
Bengourina.rida@yahoo.fr

A. Khoudiri
LAADI Laboratory
Faculty of Science and Technology
University of Djelfa
Djelfa, Algeria
a.khoudiri@yahoo.fr

Mohamed Boudiaf
LAADI Laboratory
Faculty of Science and Technology
University of Djelfa
Djelfa, Algeria
m.boudiaf@univ-djelfa.dz

*Received: 17 December 2021 | Revised: 16 January 2022 | Accepted: 21 January 2022*

**Abstract-Even though the PI controller is among the most widespread controllers in photovoltaic (PV) systems, it presents overshoots and undershoots in the tracking trajectory mode. This major disadvantage remains an open problem. In the current paper, a Direct Power Control (DPC) of a three-phase grid-connected PV system based on a Variable Gain PI (VGPI) controller is developed to remove the overshoots and undershoots in the classical PI controller. The proposed control system has been tested in the Matlab/Simulink environment. The simulation results demonstrate the feasibility and robustness of the proposed method in terms of overshoots, undershoots, and current quality.**

***Keywords-photovolatic system; direct power control; VGPI controller; overshoots; undershoots***

## I. INTRODUCTION

The high growth rate of photovoltaic (PV) systems over the last several years allows them to play a more important role in the future mixed power grid [1]. However, the cost of PV systems must be reduced further in order to increase the level of their penetration and to make the PV power plant eligible as compared to conventional energy [2]. Most PV systems are connected to the distribution grid, where the inverter is receiving increased interest in order to generate power [3]. Many control structures for grid associated PV systems have been developed thanks to the advanced development of power electronics technology and the digitization of PV systems. These control structures have the same goals, but with different principles of operation. They can generally be divided into two categories, the control loops of powers and currents. Direct Power Control (DPC) is a kind of high-performance control structure for grid connected PV systems based on active and reactive power similar to the conventional Direct Torque Control (DTC) strategy for electrical machines [4]. In the classical structure of DPC, a PI controller is used for controlling the DC bus voltage. These organs are of general use in many applications because they have simple design and easy tuning parameters [5]. However, the PI controllers have problems in removing the overshoots and undershoot in the tracking trajectory of continuous power as it is affected by solar radiation. This problem is due to the controller parameters which are constant. This is why the idea of designing a variable gain regulator has been proposed to overcome this trade off. A VGPI controller can be seen as a generalization of a classical PI controller with the proportional and integrator gains varying

Corresponding author: Boukhalfa Mohamed

along a tuning curve [6]. Several authors have chosen to solve the problem with other methods such as: non-linear approaches [7, 8], Fuzzy Logic controllers [9, 10], Artificial Neural Networks (ANNs) [11], and metaheuristic optimization [12, 13]. However, these solutions are complex and not appreciated by the industry. In this paper, a VGPI regulator is proposed to replace the PI regulator to control the DC bus voltage of the grid connected PV inverter. A detailed study of the coordinated control between the DPC control and the VGPI controller is given. Simulations on a 3.7kW two-stage PV system are performed in order to check the effectiveness of the DPC based on the proposed topology under several test conditions.

## II. CONTROL STRUCTURE OF TWO-STAGE THREE-PHASE GRID-CONNECTED PV SYSTEMS

### *A. System Overview*

The proposed conversion system is shown in Figure 1. It consists of two stage grid associated PV systems. Two main tasks should be achieved by the grid associated PV inverters: (1) Maximum Power Point Tracking (MPPT) control to extract the maximum power provided by the PV panels and (2) the injection of grid current with high power quality.

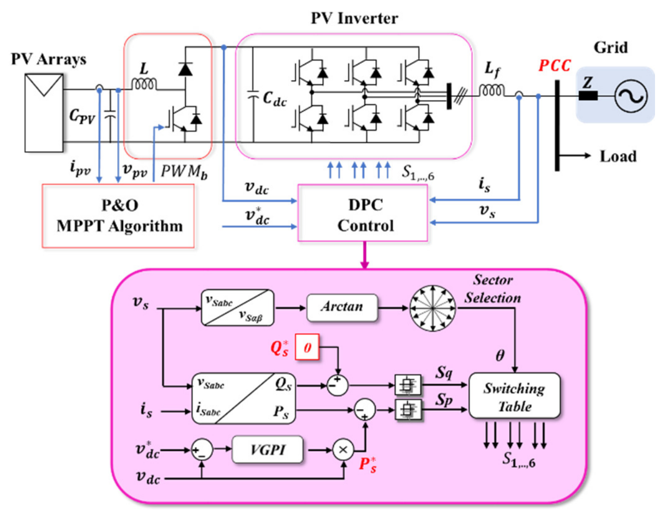


Fig. 1. Three-phase grid associated PV system with P&O MPPT and DPC control based on a VGPI controller.

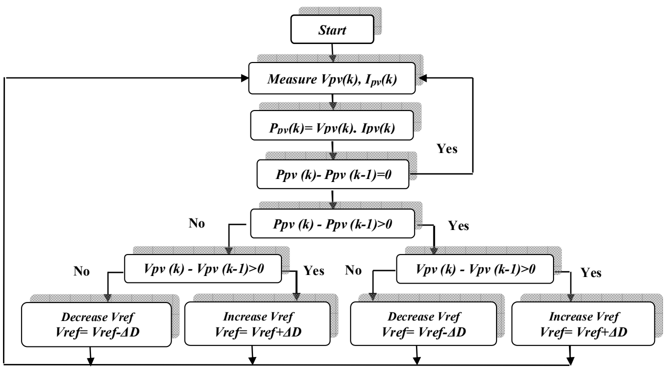


Fig. 2. Flowchart of the P&O MPPT algorithm.

### *B. Boost Converter Controller*

The boost converter controls the maximum power output using MPPT control. The MPPT algorithm is implemented in the boost converter. Hill-climbing and fractional methods are widely adopted in PV systems. Perturb and Observe (P&O) is a type of hill-climbing method consisting of a continuous reference voltage search process to reach the Maximum Power Point (MPP) [14]. The principle of P&O is depicted in the flowchart in Figure 2.

### *C. Lookup Table Based Direct Power Control*

DPC for grid associated inverters was developed to have control on the instantaneous active and reactive power directly by selecting the optimum switching state of the converter, which was first proposed in [15] and more clearly presented in [16]. The main principle of DPC is similar to DTC in motor drives [17]. It directly selects the desired voltage vector from a predefined switching table, according to the grid voltage position (or virtual flux position) and the errors between the reference active/reactive power and feedback value. The control structure of a typical DPC is represented in Figure 1. The switch table is shown in Table I. The power calculation block reads as:

$$\overline{S}_s = P_s + jQ_s \quad (1)$$

$$P_s = \frac{3}{2}(V_{s\alpha\beta}.I_{s\alpha\beta}) = \frac{3}{2}(v_{s\alpha}.i_{s\alpha} + v_{s\beta}.i_{s\beta}) \quad (2)$$

$$Q_s = \frac{3}{2}(V_{s\alpha\beta} \times I_{s\alpha\beta}) = \frac{3}{2}(v_{s\beta}.i_{s\alpha} - v_{s\alpha}.i_{s\beta}) \quad (3)$$

where: $V_{s\alpha\beta} = v_{s\alpha} + jv_{s\beta}$ and $I_{s\alpha\beta} = i_{s\alpha} + ji_{s\beta}$ .

In order to obtain the position of grid voltage vector, the angle of grid voltage can be calculated based on $v_{s\alpha}$ and $v_{s\beta}$ as:

$$\theta = arctan\left(\frac{v_{s\beta}}{v_{s\alpha}}\right) \quad (4)$$

The switch table is based on the position of the grid voltage vector. In order to optimize the performance of the converter, the grid voltage can be divided into 12 sectors. The angle of the 12 sectors can be obtained as:

$$(n-2)\frac{\pi}{6} \le \theta_n \le (n-1)\frac{\pi}{6},\ n = 1,2,....,12. \quad (5)$$

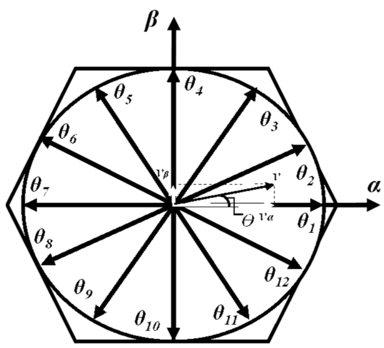


Fig. 3. Plant (α, β) divided in 12 sectors.

The power hysteresis controller consists of active power and reactive power hysteresis controllers. The input is the error between the reference and the real power. The output reflects the status of power deviation, which can be expressed as $S_p$ and $S_q$. $S_p$ and $S_q$ only have two statuses, which can be expressed as:

$$S_p = \begin{cases} 0 & P < P_{ref} - H_p \\ 1 & P > P_{ref} - H_p \end{cases} \quad (6)$$

$$S_q = \begin{cases} 0 & Q < Q_{ref} - H_q \\ 1 & Q > Q_{ref} + H_q \end{cases} \quad (7)$$

where $H_p$ and $H_q$ are the hysteresis bands.

DPC has been known as a powerful and robust control scheme for grid connected inverters, but high-power ripples and variable switching frequency are two of the most notable drawbacks of the conventional DPC. Furthermore, the required sampling frequency is usually very high in order to achieve relative satisfactory performance which increases the hardware burden and might limit the application of this method. The proposed switching table for all sectors is represented in the Table I.

TABLE I. SECTOR SWITCHING TABLE

| $S_p$ | $S_q$ | $\theta_1$ | $\theta_2$ | $\theta_3$ | $\theta_4$ | $\theta_5$ | $\theta_6$ | $\theta_7$ | $\theta_8$ | $\theta_9$ | $\theta_{10}$ | $\theta_{11}$ | $\theta_{12}$ |
|---|---|---|---|---|---|---|---|---|---|---|---|---|---|
| **1** | **1** | $v_6$ | $v_7$ | $v_1$ | $v_0$ | $v_2$ | $v_7$ | $v_3$ | $v_0$ | $v_4$ | $v_7$ | $v_5$ | $v_0$ |
| **1** | **0** | $v_7$ | $v_7$ | $v_0$ | $v_0$ | $v_7$ | $v_7$ | $v_6$ | $v_0$ | $v_5$ | $v_7$ | $v_0$ | $v_0$ |
| **0** | **1** | $v_6$ | $v_1$ | $v_1$ | $v_2$ | $v_2$ | $v_3$ | $v_3$ | $v_4$ | $v_4$ | $v_5$ | $v_5$ | $v_6$ |
| **0** | **0** | $v_1$ | $v_2$ | $v_2$ | $v_3$ | $v_3$ | $v_4$ | $v_4$ | $v_3$ | $v_3$ | $v_6$ | $v_6$ | $v_1$ |

## III. VGPI CONTROLLER

To reduce variations and instability in the DC link voltage a VGPI controller is proposed for the DC link voltage regulation. The error between the voltage of the capacitor $V_{dc}$ and the reference voltage $V_{dcref}$ are used as an input to the VGPI controller and the output is the reference active power $P_{ref}$. A VGPI controller is a most generalized classical PI controller [18] with varying gain in time along a polynomial curve. This gain attains its final value as the steady state is reached [6]. This controller with continually adapted parameters can limit overshoot during startups with a rapid load disturbance rejection. Figure 4 shows the block diagram of the VG-PI controller.

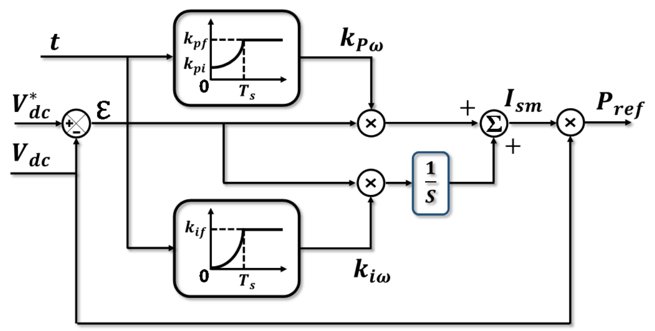


Fig. 4. Block diagram of the VGPI controller.

The speed VGPI controller delivers at its output the inverter current:

$$I_{sm} = k_{p\omega}.(V_{dcref} - V_{dc}) + k_{i\omega}.\int (V_{dcref} - V_{dc}).dt \quad (8)$$

$k_{p\omega}$, $k_{i\omega}$ are given by:

$$k_{p\omega} = \begin{cases} (k_{pf} - k_{pi})\left(\frac{t}{T_s}\right)^n + k_{pi} & if \ t < T_s \\ k_{pf} & if \ t \geq T_s \end{cases} \quad (9)$$

$$k_{i\omega} = \begin{cases} k_{if}\left(\frac{t}{T_s}\right)^n & if \ t < T_s \\ k_{if} & if \ t \geq T_s \end{cases} \quad (10)$$

where $k_{pi}$ and $k_{pf}$ are the initial and final values of the proportional gain, and $k_{if}$ is the integrator gain final value. $T_s$ and $n$ are the saturation time and the polynomial degree.

Consequently, the reference power quantity is deduced as:

$$P_{ref} = I_{sm} V_{dc} \quad (11)$$

### A. VGPI Controller Parameter Setting

The parameters are obtained by the test-error method as follows [6,18]:

- Choose a value $k_{if}$ to obtain a rapid load disturbance rejection.
- Set the degree $n$ and the saturation time $T_s$.
- Derive the values $k_{pi}$ and $k_{pf}$ so as the smallest overshoot and undershoot are obtained.
- To eliminate completely the overshoot and undershoot, increase$T_s$. If the excess is not eliminated, increase $n$.

### B. Performance Verification of the VG-PI Control

The effectiveness of the proposed control has been verified on MATLAB/Simulink. The system configuration is shown in Figure 1 and the system parameters are given in Table II.

TABLE II. PARAMETERS OF THE TWO-STAGE THREE-PHASE GRID-CONNECTED PV

| | |
|---|---|
| **PV rated power** | 3 kW |
| **Boost converter inductor** | $L$ = 6 mH |
| **PV-side capacitor** | $C_{pv}$ = 200 µF |
| **L-filter** | $L_f$= 2.5 mH |
| **Switching frequency** | Boost converter: $f_b$ = 16 kHz, |
| **DC-link voltage** | $V_{dc}$ = 450 V |
| **Grid nominal voltage (RMS)** | $V_g$ = 230 V |
| **Grid nominal frequency** | $\omega$ = 2π×50 rad/s |

First, a variable solar irradiance profile as plotted in Figure 5 has been utilized in the simulation. The solar irradiance level starts from 1000W/m$^2$, then it decreases to 400W/m$^2$ and after that it increases to 800W/m$^2$, and finally decreases to 200W/m$^2$. The PV power amounts attain their optimum theoretical values, which are respectively 3.6kW, 1.39kW, and 0.67kW, within milliseconds despite solar irradiance variations. The temperature is kept constant all time and equal to 25°C.

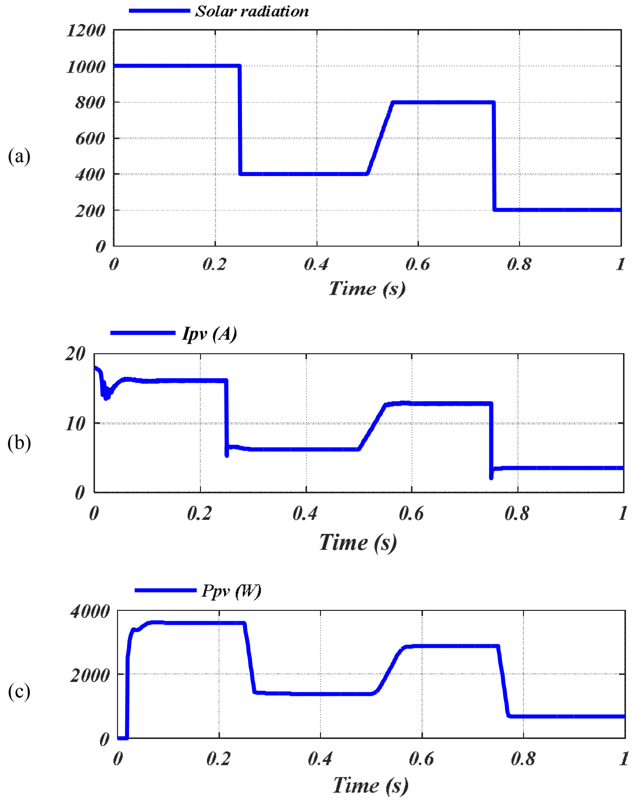


Fig. 5. (a) Solar radiation, (b) current of the PV array, and (c) PV power.

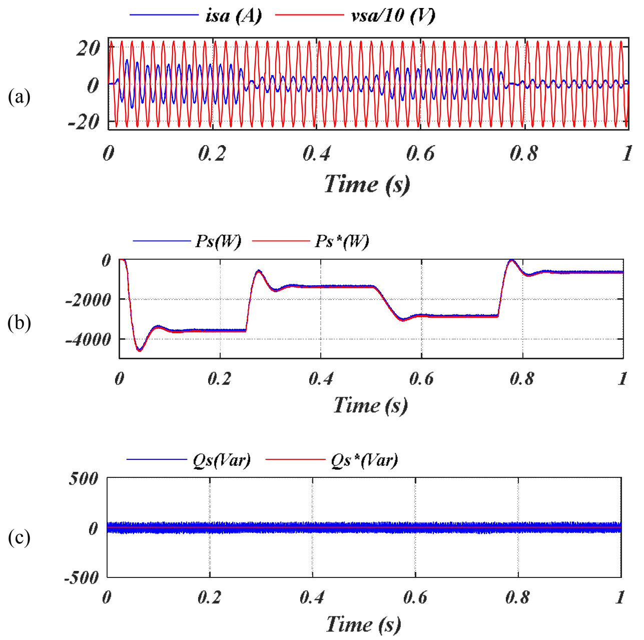


Fig. 6. Simulation results of the proposed DPC with PI Controller. (a) Grid current and voltage, (b) active power reference and response, (c) reactive power reference and response.

Figures 6 and 7 show the simulation results for systems with PI and VGPI controllers. Grid current ($i_s$), grid voltage ($v_s$), reactive power ($Q_s$), and active power ($P_s$) are depicted. The results show that the current is sinusoidal after the control application but with opposition in phase with the corresponding voltages. The negative sign of the utility active power ($P_s$) means current injection to the grid or load. The reactive power is always zero. Note that the wave chatring of active and reactive power is generally acceptable for both regulation approaches. Furthermore, a perfect decoupling is observed between active and reactive powers. By inspecting Figure 8, one can clearly see that the DC voltage perturbations at the instants of the power variation are very weak as compared to those of the PI regulator. This indicates the robustness of the VGPI approach.

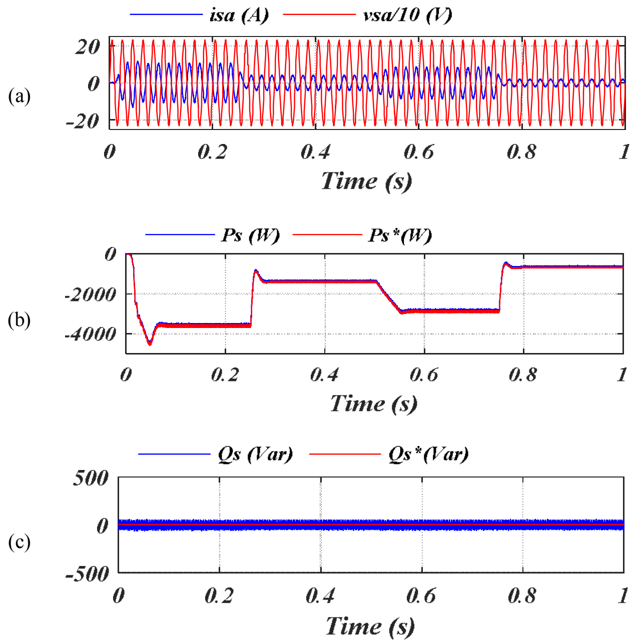


Fig. 7. Simulation results of the proposed DPC with VGPI controller. (a) Grid current and voltage, (b) active power reference and response, (c) reactive power reference and response.

Figure 9 shows the behavior of an AC current phase as a function of the solar irradiance (1000, 400, 800, 200W/m$^2$). It is worth noting that the dc-bus voltage and the instantaneous powers present good tracking to their reference values with low overshoot, undershoot and Total Harmonic Distortion (THD). This is consistent with the information reported in [19-21]. Table III summarizes the obtained values of the overshoot and undershoot stabilization time along with the THD. From this table, one can see that for each considered irradiation, the overshoot and undershoot recorded with the use of the VGPI regulator are superior than their counterparts if the PI regulator is used. Besides, the THD is less than 5% for all irradiation values being considered here. Hence, our derived THD is in accordance with the IEC 61727 and IEEE 1547 recommendations respectively.

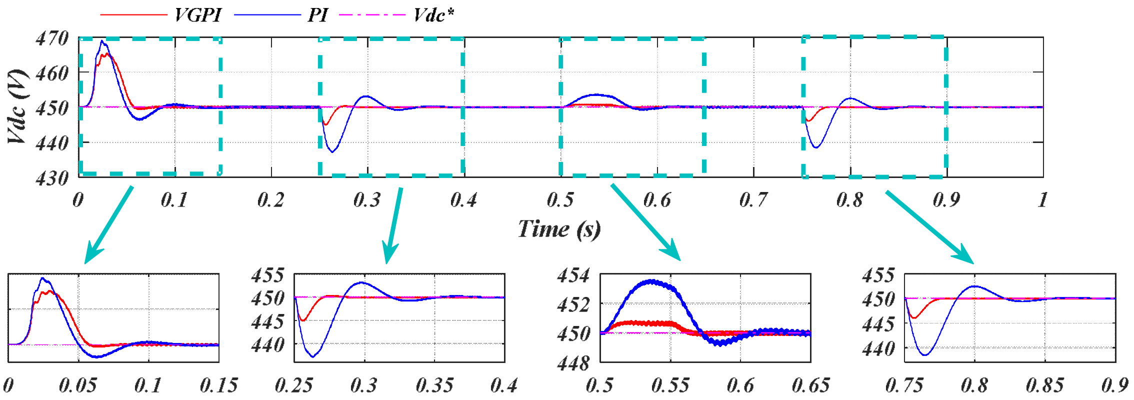


Fig. 8. DC converter voltage.

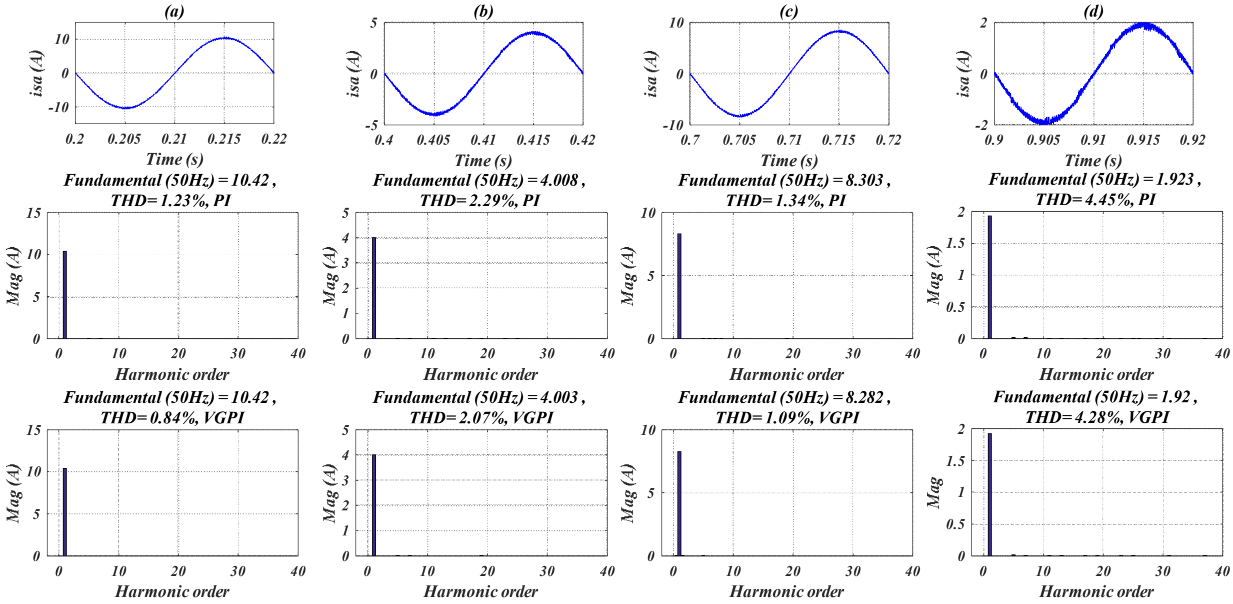


Fig. 9. Grid current and harmonic spectrum with PI and VGPI controllers.

TABLE III. COMPARATIVE STUDY

| Irradiation | Parameters | DPC-PI | DPC-VGPI |
|---|---|---|---|
| 1000 W/m$^2$ | Overshoot % | 4.22 | 3.4 |
| | Undershoot % | 0.82 | 0.155 |
| | $T_s$ (s) | 0.172 | 0.087 |
| | THD % | 1.23 | 0.84 |
| 400 W/m$^2$ | Overshoot % | 0.71 | 0.06 |
| | Undershoot % | 2.866 | 1.142 |
| | $T_s$ (s) | 0.138 | 0.044 |
| | THD % | 2.29 | 2.07 |
| 800 W/m$^2$ | Overshoot % | 0.8 | 0.066 |
| | Undershoot % | 0.2 | 0 |
| | $T_s$ (s) | 0.146 | 0.07 |
| | THD % | 1.34 | 1.09 |
| 200 W/m$^2$ | Overshoot % | 0.55 | 0 |
| | Undershoot % | 2.577 | 0.9 |
| | $T_s$ (s) | 0.136 | 0.059 |
| | THD % | 4.45 | 4.28 |

## IV. CONCLUSION

DPC control based on VGPI controller applied to a grid connected PV system has been proposed and discussed in this paper. The analysis of the obtained results shows the robustness, the effectiveness, and the good performance of the proposed VGPI controller based on the DPC strategy. This regulator outperforms the PI controller, from the point of view of the response time and follow-up of the reference values. Finally, as perspectives of this study, further efforts are to be carried out to optimize the control system with consideration of the shading effect and deep voltages grids.

## REFERENCES

[1] A. Sangwongwanich, Y. Yang, F. Blaabjerg, and H. Wang, "Benchmarking of Constant Power Generation Strategies for Single-Phase Grid-Connected Photovoltaic Systems," *IEEE Transactions on Industry Applications*, vol. 54, no. 1, pp. 447–457, Jan. 2018, https://doi.org/10.1109/TIA.2017.2740380.

[2] A. Sangwongwanich, Y. Yang, F. Blaabjerg, and D. Sera, "Delta Power Control Strategy for Multistring Grid-Connected PV Inverters," *IEEE Transactions on Industry Applications*, vol. 53, no. 4, pp. 3862–3870, Jul. 2017, https://doi.org/10.1109/TIA.2017.2681044.

[3] L. Hassaine, E. OLias, J. Quintero, and V. Salas, "Overview of power inverter topologies and control structures for grid connected photovoltaic systems," *Renewable and Sustainable Energy Reviews*, vol. 30, pp. 796–807, Oct. 2014, https://doi.org/10.1016/j.rser.2013.11.005.

[4] K. Kulikowski and A. Sikorski, "Comparison of new DPC methods for two- and three-level AC/DC converters," in *2010 International School on Nonsinusoidal Currents and Compensation*, Lagow, Poland, Jun. 2010, pp. 156–161, https://doi.org/10.1109/ISNCC.2010.5524497.

[5] A. Mechernene, L. Chrifi Alaoui, M. Zerikat, N. Benharir, and H. Benderradji, "VGPI controller for high performance speed tracking of induction motor drive," in *3rd International Conference on Systems and Control*, Jul. 2013, pp. 472–477, https://doi.org/10.1109/ICoSC.2013.6750901.

[6] A. Miloudi, E. Al-Radadi, and A. Draou, "A variable gain PI controller used for speed control of a direct torque neuro fuzzy controlled induction machine drive," *Turkish Journal of Electrical Engineering*, vol. 15, no. 1, pp. 37–49, Nov. 2007.

[7] R.-J. Wai, "Adaptive sliding-mode control for induction servomotor drive," *IEE Proceedings - Electric Power Applications*, vol. 147, no. 6, pp. 553–562, Nov. 2000, https://doi.org/10.1049/ip-epa:20000628.

[8] O. Benzineb, H. Salhi, M. Tadjine, M. S. Boucherit, and M. Benbouzid, "A PI/Backstepping Approach for Induction Motor Drives Robust Control," *International Review of Electrical Engineering*, vol. 5, no. 2, pp. 426–432, Dec. 2010.

[9] I. Sefa, N. Altin, S. Ozdemir, and O. Kaplan, "Fuzzy PI controlled inverter for grid interactive renewable energy systems," *IET Renewable Power Generation*, vol. 9, no. 7, pp. 729–738, 2015, https://doi.org/10.1049/iet-rpg.2014.0404.

[10] I. Abadlia, L. Hassaine, A. Beddar, F. Abdoune, and M. R. Bengourina, "Adaptive fuzzy control with an optimization by using genetic algorithms for grid connected a hybrid photovoltaic–hydrogen generation system," *International Journal of Hydrogen Energy*, vol. 45, no. 43, pp. 22589–22599, Jun. 2020, https://doi.org/10.1016/j.ijhydene.2020.06.168.

[11] Y. Sun, S. Li, B. Lin, X. Fu, M. Ramezani, and I. Jaithwa, "Artificial Neural Network for Control and Grid Integration of Residential Solar Photovoltaic Systems," *IEEE Transactions on Sustainable Energy*, vol. 8, no. 4, pp. 1484–1495, Jul. 2017, https://doi.org/10.1109/TSTE.2017.2691669.

[12] B. M. Rida, M. Rahli, S. Slami, and L. Hassaine, "PSO based Direct Power Control for a Multifunctional Grid Connected Photovoltaic System," *International Journal of Power Electronics and Drive Systems*, vol. 9, no. 2, pp. 610–621, Jun. 2018, https://doi.org/10.11591/ijpeds.v9.i2.pp610-621.

[13] C.-H. Liu and Y.-Y. Hsu, "Design of a Self-Tuning PI Controller for a STATCOM Using Particle Swarm Optimization," *IEEE Transactions on Industrial Electronics*, vol. 57, no. 2, pp. 702–715, Oct. 2010, https://doi.org/10.1109/TIE.2009.2028350.

[14] N. Femia, D. Granozio, G. Petrone, G. Spagnuolo, and M. Vitelli, "Predictive amp; Adaptive MPPT Perturb and Observe Method," *IEEE Transactions on Aerospace and Electronic Systems*, vol. 43, no. 3, pp. 934–950, Jul. 2007, https://doi.org/10.1109/TAES.2007.4383584.

[15] T. Ohnishi, "Three phase PWM converter/inverter by means of instantaneous active and reactive power control," in *Control and Instrumentation Proceedings IECON '91: 1991 International Conference on Industrial Electronics*, Jul. 1991, vol. 1, pp. 819–824, https://doi.org/10.1109/IECON.1991.239183.

[16] T. Noguchi, H. Tomiki, S. Kondo, and I. Takahashi, "Direct power control of PWM converter without power-source voltage sensors," *IEEE Transactions on Industry Applications*, vol. 34, no. 3, pp. 473–479, Feb. 1998, https://doi.org/10.1109/28.673716.

[17] R. Datta and V. T. Ranganathan, "Direct power control of grid-connected wound rotor induction machine without rotor position sensors," *IEEE Transactions on Power Electronics*, vol. 16, no. 3, pp. 390–399, Feb. 2001, https://doi.org/10.1109/63.923772.

[18] A. Miloudi, E. A. A. Radadi, A. Draou, and Y. Miloud, "Simulation and modelling of a variable gain PI controller for speed control of a direct torque neuro fuzzy controlled induction machine drive," in *2004 IEEE 35th Annual Power Electronics Specialists Conference (IEEE Cat. No.04CH37551)*, Aachen, Germany, Jun. 2004, vol. 5, pp. 3493-3498, https://doi.org/10.1109/PESC.2004.1355092.

[19] S. Saad, "Enhancement of Solar Cell Modeling with MPPT Command Practice with an Electronic Edge Filter," *Engineering, Technology & Applied Science Research*, vol. 11, no. 4, pp. 7501–7507, Aug. 2021, https://doi.org/10.48084/etasr.4304.

[20] S. Hota, M. K. Sahu, and J. M. R. Malla, "A Standalone PV System with a Hybrid P&O MPPT Optimization Technique," *Engineering, Technology & Applied Science Research*, vol. 7, no. 6, pp. 2109–2112, Dec. 2017, https://doi.org/10.48084/etasr.1374.

[21] B. Korich, A. Benaissa, B. Rabhi, and D. Bakria, "A Novel MPPT Design for a Partially Shaded PV System Using Spotted Hyena Optimization Algorithm," *Engineering, Technology & Applied Science Research*, vol. 11, no. 6, pp. 7776–7781, Dec. 2021, https://doi.org/10.48084/etasr.4490.